Modeling and Simulation of Electromutagenic Processes for Multiscale Modification of Concrete

Jinko Kanno[1], Nicholas Richardson[1], James Phillips[1],Kunal Kupwade-Patil[3], Daniela S. Mainardi[2] and Henry E. Cardenas[3],

[1]Mathematics and Statistics Program, Louisiana Tech University, Ruston, LA 71272, U. S. A.

[2]Chemical Engineering Program/Institute for Micromanufacturing, Louisiana Tech University

[3]Mechanical Engineering Program, Louisiana Tech University

ABSTRACT

Concrete contains numerous pores that allow degradation when chloride ions migrate through these paths and make contact with the steel reinforcement in a structure. Chlorides come mainly from the sea or de-icing salts. To keep the reinforcement from being exposed to chlorides, it is possible to electrokinetically force nanoparticles into the pores, blocking access. This procedure is called electrokinetic nanoparticle treatment. When the particles used are reactive in nature, the process becomes both structural and chemical in nature. We use the term electromutagenic processing to describe such extensive electrochemical remodeling. Filling the pores in a block of concrete with solid materials or nanoparticles tends to improve the strength significantly. In this paper, results obtained from modeling and simulation were aimed at multi-scale porosity reduction of concrete. Since nanoparticles and pores were modeled with spheres and cylinders having different sizes, the results were compared with traditional sphere packing problems in mathematics. There were significant differences observed related to the sizes of spheres and allowable boundary conditions. From traditional sphere packing analysis the highest porosity reduction anticipated was 74%. In contrast, the highest pore reduction obtained in this work was approximately 50%, which matched results from actual electrokinetic nanoparticle treatments. This work also compared the analytical and simulation methods used for several sizes of nanoparticles and pores.

Keywords: Simulation, Modeling, Particle Packing, Porosity

1. INTRODUCTION

In 2001, the U.S. Federal Highway Administration, in concert with CC Technologies Laboratories Inc., finalized a landmark study on the direct costs of corrosion in nearly every major U.S. industrial sector [1]. Corrosion in bridge structures is a global problem. The study found that the annual direct cost of highway bridge repairs (largely related to reinforcement corrosion) was $8.3 billion in the U.S. alone. The proposed electrokinetic approach will provide a radical increase in the durability of concrete repairs by removing aggressive chemical species and sealing the region with a close chemical relative of the original cement binder material in ordinary Portland cement. Such a treatment may provide a sound foundation for application of traditional repair materials that would otherwise be undermined by continued reinforcement corrosion. An adaptation of this technology could become a cost-effective repair method for bridges, basements and other structures. Unlike a typical coating, pozzolonic nanoparticles penetrate almost as deeply as desired with a minimal electric field as small as 1 Volt/inch and a current draw of less than 0.1 Amperes per square foot. The electric field provides a targeted treatment that eventually could be applied with a paint roller (adapted to apply a voltage) and go preferentially to where the porosity, cracking and steel reinforcement is most needful of remedy. Conventional coatings do not provide this efficiency since they must be applied evenly over the entire surface to ensure coverage.

Concrete contains numerous pores that allow corrosion when chloride ions travel through the pores and make contact with the metal reinforcement in a concrete building or bridge. Chlorides come mainly from marine environments and de-icing salts applied to roads in cold climates. To block ingress of chlorides, nanoparticles can be driven electrokinetically into the concrete pores. This procedure is called the electrokinetic nanoparticle treatment. Replacing water in pores with nanoparticles has also been shown improve the compressive strength and the tensile strength of the material. Inside concrete, the elevated pH causes the steel reinforcement to develop a passive oxide film that effectively protects it against corrosion. The reduction of this pH or the introduction of aggressive chemical species, such as chlorides, can cause this passive film to be disrupted, permitting corrosion to take place [2][3][4][5][6][7].

Chloride ions become available due to the application of de-icing salts, exposure to marine environments or even the usage of coastal sand. The chloride ion causes rapid corrosion of steel bars in concrete [8]. A major issue here is that the chloride ion is not consumed in the corrosion process [9]. It acts as a reaction catalyst that is continuously recycled. For this reason, many concrete repairs continue to suffer from corrosion because the repair failed to reduce the chloride content of the structure. With the chlorides eliminated, or at least reduced in concentration as compared to the pH, the life of a properly repaired structure is significantly extended [10].

Durability problems commonly occur when porosity is too high [11]. There are some remedies that can be applied to reduce permeability at the surface of a structure. Water seepage through cementitious materials is addressed using polymer coatings, reactive organic and inorganic grouts, and application of pulsed electric current [11][12][13][14]. Electric current is occasionally used to induce electro-osmosis in the direction opposing seepage flow in a basement structure [15][16].

When used either as partial replacements or as mix additions to Portland cement, silica fume (SF) and fly ash are well recognized for reducing the permeability and increasing the strength of concrete [17][18][19]. This modification must take place at the time that the concrete is mixed. These silica and alumina containing additions react with calcium hydroxide within the concrete and so provide a reduction in porosity of concrete as the material ages.

Colloidal silica and sodium silicate have also been used to improve the permeabilty of cementitious materials. Some researchers have investigated the addition of these agents as partial cement and water replacements during the mix. Chandra found that, because of the finer size of the colloidal silica, this material exhibits faster reactivity than SF [20]. Nelson investigated the pozzolonic reactivity of colloidal silica and quaternary ammonium silicate in Portland cement pastes [21]. This work showed higher strengths than plain concrete for 150 days after the batch. Campillo studied the influence of nanoscale colloidal silica on cement properties [22]. Improved compression strength was observed. The reason cited for

strength improvement is that reaction products are formed within the pores, reducing porosity.

Another means of reducing porosity or at least blocking pores is by using an electric field to transport passive or reactive species into a water-saturated, porous medium. A paper manufacturing process patented in Europe involves the electrokinetic transport of reactive pore blocking agents that chemically react with some elements of the flow path [23]. This process influences the pore structure and the chemistry of the paper. Similar concepts directed toward seepage control crack repair were found to achieve some success in reducing the permeability of damaged concrete [24][25][26]. Other work examined mixtures of silica fume and calcium hydroxide as a mechanically applied crack repair agent [27].

2. PROCEDURES

In this work nanoparticles and pores were modeled with spheres and cylinders having different sizes so that our problems can be compared with traditional sphere packing problems. In the following sections the analytical particle assembly modeling, molecular modeling, and computer simulation work are described.

Analytical modeling

In the analytical modeling nanoparticles and pores were modeled by spheres and cylinders having multiple sizes. In this approach the cylinders were visualized in the 3-dimensional xyz-space where the base of cylinder was in xy-plane and height was measured in the z-axis direction. Both stacking and packing assembly methods were applied in the analytical model. The nanoparticles were placed in an order selected to minimize calculation complexity. The packing method was used to place nanoparticles or spheres horizontally and the stacking method was used to place them vertically. A crystallographic packing method was not used because it was inconsistent with the boundary conditions of the system. This boundary condition constrains all spheres to be inside of cylindrical pores. This is a significant difference from traditional sphere packing problems in which the boundaries of a unit cell are permitted to pass through individual spheres [28][29]. The highest possible packing density of monosized spheres with a sphere-crossing boundary is 0.74. In contrast multi-sized sphere packing assemblies that are bounded by multi-sized cylinders were expected to exhibit significantly lower packing densities. Analytical modeling is further detailed in the following sections.

Consider a cylinder with a circular base of diameter D and height or length L, called an *L-cylinder.* Similarly, we refer to a sphere having diameter a, b, or c with a > b > c, as *a-sphere, b-sphere,* or *c-sphere,* respectively. The procedure to approximate the numbers of *a*-spheres, *b*-spheres and *c*-spheres in the cylinder is relatively simple. The first stage was to focus on the horizontal packing within the *a-cylinder* using the *a-sphere, b-sphere,* or *c-sphere* etc. Secondly, the *a-cylinders were stacked.*

To pack *a*-spheres into an *a*-cylinder the 'hexagonal lattice packing' approach was used. In this approach each sphere touched six other spheres horizontally. Since the available packing space is bound by a cylindrical border, this approach was used as much as possible until no further a-spheres would fit. The rest of the procedure follows what could be described as a *modified hexagonal lattice packing method.* More precisely, this approach used the projection of the *a*-spheres onto the cylindrical base. This reduced the problem to a 2-dimensional

geometry. Gaps remaining between the cylinder border and the *a-sphere* assembly were filled with *b-spheres* and *c-spheres.*

The next step was the preparation of several equivalently packed *a*-cylinders. They were constructed in the same manner as described above. Several of these packed *a*-cylinders were assembled into the larger *L*-cylinder. This fills the cylinder to the extent of the integer value *m* which is obtained by discarding decimal component when *L* is divided by *a.* At this point a small reminder of the cylinder is still not filled. This remainder section or *r*-cylinder is now filled using either the *b*-spheres or the *c*-spheres by using the modified hexagonal packing method.

Molecular modeling

Applied quantum chemical methods [30][31] such as Ab Initio methods [32], Density Functional Theory (DFT) [33][34], and semi-empirical methods [35][36], have been successfully used for getting information about the geometrics and energetics of atomic and molecular systems, activation energies, and reaction mechanisms [31]. DFT incorporates electron correlation, which is neglected in the simplest ab initio methods such as Hartree-Fock, at a similar computational cost [37]. DFT provides a relatively efficient tool with which to compute the ground state energy in realistic models of clusters and bulk materials.

Density Functional Theory (DFT) calculations were performed using the DMOL3 module of the Materials Studio® developed by Accelrys, Inc. The density functional employed in these calculations is the non-local Generalized Gradient Approximation (GGA) exchange-correlation functional of Perdew and Wang, PW91 [38]. This method was used in combination with the Double Numerical plus polarization (DNP) basis set, which includes one atomic orbital for each occupied atomic orbital, a second set of valence atomic orbitals,
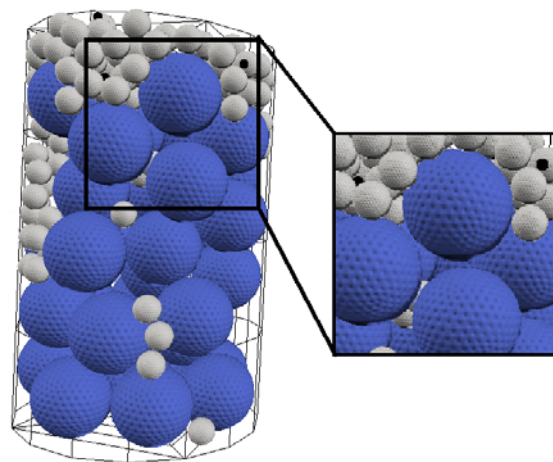

Figure 1. A packing simulation output showing 6 nanometer particles (dark) and 2 nanometer particles (white). The solvated chloride ions are black.

a polarization *d*-function on all non-hydrogen atoms and a polarization *p*-function on all hydrogen atoms. Geometry optimizations and harmonic vibrational frequency calculations were performed to ensure that stationary points on the Potential Energy Surface of the clusters were in fact local minima. Spin multiplicity (2S+1) states were checked in all calculations and ground state geometries presented. When this theory level is used, errors are expected to be in the 2nd decimal for calculated bond lengths in Angstroms, Å (1Å = 0.1 nanometer) [31].

Transport Simulation Model with Molecular Modeling Rules

The simulation used a cylinder to represent a pore of a certain size and spheres to represent nanoparticles that were being inserted to reduce the pore volume. The simulation was designed to show changes in porosity as particles were being added to the system. During the simulation, these particles were constrained to follow simple chemical collision rules. The first rule was that each particle must be completely inside the cylinder. This means that if any part of the particle violated the cylindrical wall it could not be used in calculating the porosity reduction and was thus removed. Also each particle was not permitted to intersect with any other particle. These collisions were tested continuously by using the position and radius of the particles and the radius of the cylinder.

Two types of motion were simulated. First there was a simple drift velocity along the cylinder. A finite displacement was defined for the distance that a particle was to move per unit of time and per simulation cycle. During the drift motion, the simulation checked up to nine positions in the flow direction to see if the particle could move without violating the space of another particle or the cylindrical wall. If the current direction of drift violated a space rule then the position that did not violate a collision rule was chosen for the direction of subsequent travel. New travel directions were chosen randomly. See Figure 1.

During the simulation, the largest size particles were added first, then the smaller size particles were added. Porosity reduction is calculated as the volume of added particles divided by the cylinder volume. The simulation is capable of adding chloride ions and determining the percentage of chlorides stopped.

Empirical Testing

Chloride ion penetration was examined experimental using 3 in diameter by 6 inch length specimens of Portland cement concrete. The type I Portland cement composition used in this work as reported by Lone Star Industries, Cape Girardeau, MO is 20.5% SiO_2, 5.21% Al_2O_3, 1.71% Fe_2O_3, 62.63% CaO, 3.83% MgO, and 3.08% SO_3. The batch composition is water 18.5 lb (8.3kg), Gravel 93.5 lb (42.4kg), Cement 36.5 lb (16.5kg), and Sand 56.5 lb (25.6kg).

Each specimen was cast with a ¼ inch diameter rod of 1018 carbon steel embedded in the center of each cylinder. Following 7 day period of exposure to salt water the specimens were subjected to chloride extraction for a period of 7 days. The extraction process was combined with nanoparticle injection for an additional 7 days.

The particle used in this study was a 20 nm diameter sphere of silica coated with a layer of 2 nm spheres of alumina. The composite spheres were suspended in a 12 volume percent fluid with a pH of 3.5. The particles carried a positive charge which made it possible to drive them into the concrete without causing the embedded steel to corrode during the injection process. See Figure 2. The intent of the particle injection process is to develop a dense layer of particles adhering directly to the steel reinforcement. Treatments were conducted for a period of 7 days. Following treatment, the specimens were re-exposed to salt water for a period of thirty days. Following the 30 day exposure period the specimens were broken open to examine the condition of the steel reinforcement. Several control specimens that were not provided with a particle treatment were also exposed to salt water and broken for comparison. The amount of corrosion products present on each bar was measured and averaged over 6 trials. These trials were compared to 5 trials for which no treatment was provided. This test was conducted to determine if the treatment could block the migration of chloride ions so that they could not cause corrosion of the steel reinforcement bars.
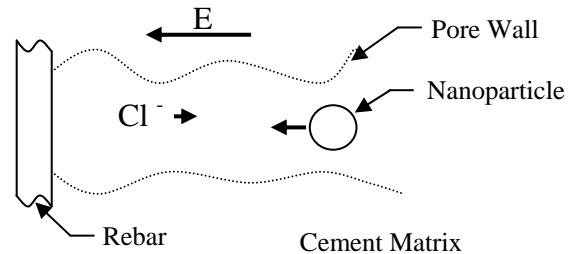

Figure 2. Reactive Electrokinetic Treatment in Cement Matrix

In other testing smaller cylinders (2 inch diameter by 4 inch height) were subjected to various combinations of nanoparticles and ions driven into the concrete. The intent of these treatments was to have phases form that could significantly reduce porosity and radically change the microstructure and strength, thus yielding an electromutagenic response. The treatments were conducted over periods that range from either 7 or 14 days. A given treatment would involve delivery of two oppositely charged particle or ion species, each deployed from opposite ends of the specimen. This arrangement would permit the formation of new phases and deep porosity reduction.

3. RESULTS

This work compared results from molecular modeling and dynamic transport to experimental results. The following sections summarize these findings.

Size of solvated chloride ion

The coordination of a Cl^- ion in the presence of two water molecules, $Cl^-(H_2O)_2$, was first investigated to provide insight into the microsolvation of Cl^- and the size of the solvated ion. In order to model fully solvated structures, systems of $Cl^-(H_2O)_{21}$ and $Cl^-_2(H_2O)_{44}$ were also studied to shed light into the likely behavior of the bulk solution.

Calculated ground state configurations are shown in Figure 3 and relevant bond lengths are listed in Table 1. Using the atomic radius of oxygen as 0.0152 nanometers (nm) and assuming a spherical shell of water molecules around the ion (first solvation shell), the calculated radius of the solvated Cl^- ion is R = 0.32 nm (Figure 3a) for the Cl^-/water system containing just 2 water molecules, and R~0.34 nm (Figure 3b and c) for the Cl^-/water systems containing 21 and 44 water molecules. From these calculations, the average distance between the Cl^- ion and the nearest H neighbor was 0.211, 0.228 and 0.230 nm for $Cl^-(H_2O)_2$, $Cl^-(H_2O)_{21}$ and $Cl^-_2(H_2O)_{44}$ respectively. By comparison, studies in the literature of the first Cl^- solvation shell of HCl in water showed a distance between the Cl^- ion and the nearest H neighbor of 0.21 nm [39].

Table 1
Coordination and radius (R) of solvated Cl⁻ ion at the PW91/DNP theory level

Bond Length (nm)	$Cl^-(H_2O)_2$	$Cl^-(H_2O)_{21}$	$Cl^-_2(H_2O)_{44}$
Cl^- - Cl^-			1.222
Average Cl^- - H (first neighbors)	0.211	0.228	0.230
Average Cl^- - O (first neighbors)	0.308	0.326	0.323
R	**0.323**	**0.341**	**0.338**

Transport simulation

From several simulations with different pore sizes and particle sizes, the porosity was usually reduced up to 50% given that the particles exhibited a good fit in the pores. This reduction was smaller than the theoretical maximum density. The theoretical value allowed partial particles to be counted in the density, which would violate the space rules of the simulation. The simulation tended to produce gaps where a partial particle would otherwise not be allowed.
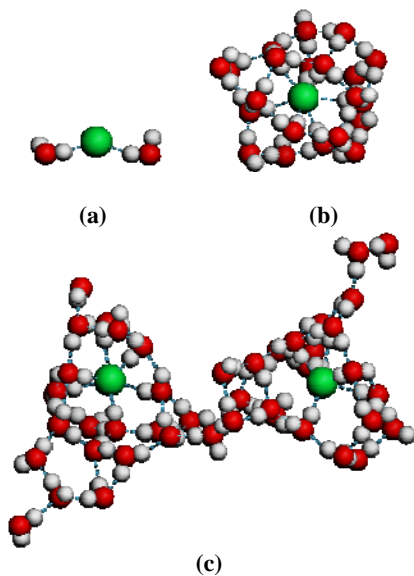

Figure 3. Ground state configurations of **(a)** $Cl^-(H_2O)_2$, **(b)** $Cl^-(H_2O)_{21}$ and **(c)** $Cl^-_2(H_2O)_{44}$ obtained at the PW91/DNP GGA DFT level. Cl⁻ (gray), hydrogen (white), oxygen (black). Dotted lines indicate hydrogen bonds.
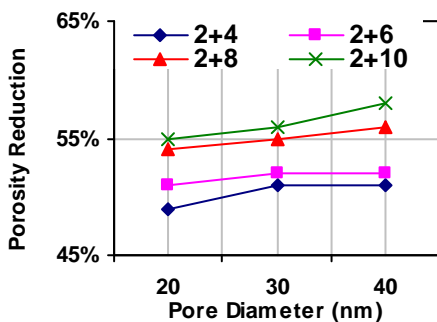

Figure 4. Simulation Data Porosity Reduction

Table 2
Analytical Stacking Compared to Simulated Packing of Pores Modeled as Cylinders of 50 nm DIA and 20 nm Height

Diameters of Particles	Particle Counts (Particle 1+particle 2 =total)	Porosity Reduction
2 & 20	544 +4=548	48%
2 & 16	994+7=1001	49%
2 & 10	1068+34=1102	57%
2 & 8	2290+48=2338	57%
2 & 6[1]	1348+138=1486	54%
2 & 6.7& 20	272+8+4=284	49%
2 & 4 & 6[2]	1252+18+138=1408	55%
2 & 4	720+455=1175	46%

1. Simulation result: 852+156=1008   54%
2. Simulation result: 414+62+152 = 628   54%

Table 3
Analytical Stacking Compared to Simulated Packing of Pores Modeled as Cylinders of 20 nm DIA and 20 nm Height

Diameters of Particles	Number of Particles	Porosity Reduction
2&10	188+4=192	46%
	359+4=363	55%
2&8	138+8=146	43%
	285+8=293	53%
2&4&6	28+38+14=80	47%
	65+13+21=99	49%
2 & 6	103+21=124	45%
	191+22=213	51%
2 & 4	122+76=198	49%
	76+83=159	49%

*Simulation packing results are shaded

Experimental corrosion and porosity findings

Following nanoparticle treatment and 30 days of re-exposure to saltwater, the specimens were broken and examined to determine extend of corrosion product formation. See Figure 5. The treated specimens are shown in Figure (b). On average these exhibited a small amount of corrosion, ~2 % of the surface area. The untreated controls exhibited a much higher corrosion rate during which over 90% of the specimens were covered with corrosion products. The controls also suffered a mass lost 15%.

In other experiments several combinations of positive and negative species were electrokinetically transported into 3 inch by 6 cylinders of concrete. The treatments were dosed such that the particles occupy would occupy all the available pore volume of the specimens. In the first 3 cases, the porosity reduction due to treatment ranged from 51 to 60%. The last case involving alumina coated exhibited a porosity reduction of 32%.
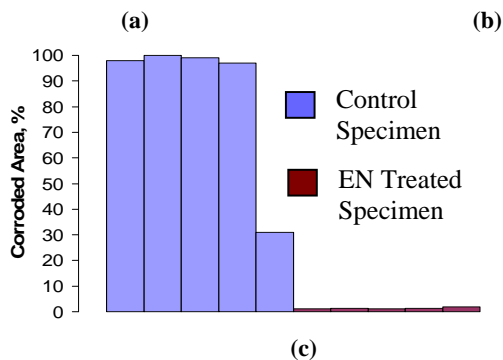
(a)   (b)

(c)

Figure 5. (a) Image of 1018 steel removed from Control Specimen. **(b)** Image of 1018 steel bars removed from EN Treated Specimen. **(c)** Column Chart of Corroded Area for Case 3 (Direct Flow current and severe Saltwater Exposure)

Table 4
Porosity Reduction due to Electrokinetic Treatment Applied to Portland Cement

Treatment	Duration (days)	Porosity Reduction (%)
SS+CH	7	51
Treatment Description: Conducted using sodium silicate and calcium hydroxide		
(SS+CH)+(ACRYLIC +AL)	14	60
Treatment Description: Conducted with two different sets of liquids sodium silicate, calcium hydroxide and acrylic co-polymer and alumina coated silica alternating the sets of fluids every 2 days		
ACRYLIC+AL	7	54
Treatment Description: Conducted with acrylic co-polymer and alumina coated silica for 7days		
AL+CH	7	32
Treatment Description: Conducted with alumina coated silica and calcium hydroxide for 7 days		

3. DISCUSSION

When conducting molecular modeling, as the number of atoms in the system increases, simulations must implement a compromise between accuracy of results and ease of computation. As the atom cluster grew, the total water-water interaction became more competitive with the total ion-water interaction, and therefore hydrogen bonding among water molecules played a significant role in determining the optimal configurations of the various ion-water clusters.

From the Density Functional Theory simulations conducted at the PW91/DNP theory level, the calculated size of the solvated

Cl$^-$ ion suggested for further mathematical modeling was R=0.34 nm, corresponding to the radius of the particle representing the chloride ion. This value was selected based on extended calculations involving systems containing 1 Cl$^-$ ion and 21 and 44 water molecules (Figures 3b and c) for which the same radius of the first chloride salvation shell was obtained, and therefore its size confirmed.

In the empirical corrosion work, the alumina coated silica particles are surrounded by 2 nm particles of alumina. After the particles became lodged somewhere in the pore structure the electric field can cause these small particles to separate from the silica particle and form a cluster of smaller particles. The interparticle spacing of these 2 nm clusters is estimated to be approximately 0.4 nm. As noted above, the smallest solvated chloride ion was expected to be ~0.64 nm which is larger than the interparticle spacing among the alumina particles. The molecular model indicates that the cluster of alumina particles was expected to form a barrier to chloride penetration. The experimental results indicate that the treated specimens did not suffer from chloride induced corrosion. These findings indicate that the molecular model predicted correctly that the electrokinetic treatment using alumina coated silica nanoparticles would protect the steel reinforcement from chloride induced corrosion.

One of the goals in this study was to find efficient size ratios of two or three nanoparticle diameter combinations for reducing porosity. The analytical and simulation results provided a comparison between stacking and packing assembly. As expected the packing method tended to provide greater or equal porosity reduction (See Table 3). The size ratio 1:2 showed no difference between the assembly methods. Interestingly, the packing simulation showed the most porosity reduction in the size ratio 1: 5 for both the packing simulation and the stacking analytical method (Table 2 and Table 3).

In all analytical and simulation cases considered the greatest porosity reduction achieve was approximately 57%. By comparison the greatest porosity reduction achieved among the empirical results as 60%. In general, the simulation and model predicted a saturating particle treatment would achieve a porosity reduction in the vicinity of 50%. This nominal 50% values was typically achieved in the experimental results as well. These findings indicate that the simulation as well as the analytical models successfully predicted the porosity reduction of a particle saturating treatment.

The current simulation runs in quadratic time. The next generation simulation will significantly reduce the asymptotic complexity of the problem so that the average run-time will be linear in regard to cylinder length. The next generation simulation is still in testing, but is showing promising results. Fine grain parallelization may also be utilized to decrease the runtime of a single simulation on a multi-processor architecture. The next version will also use statistical analysis to determine if adding transport rules such as Van Der Waals force interaction constraints or modifying other parameters will improve performance.

4. CONCLUSIONS

From the Density Functional Theory simulations the calculated radius of the solvated Cl$^-$ ion was 0.34 nm. In general, both the simulation and analytical model predicted that a saturating particle treatment would achieve a porosity reduction in the vicinity of 50% (regardless of particle size). This nominal 50%

value was typically achieved in the experimental results as well. The simulation also showed that the greatest porosity reduction (57%) was achieved with a particle size ratio of 1:5 for both the packing simulation and the stacking analytical method. Both the molecular model and the simulation predicted correctly that the electrokinetic treatment using alumina coated silica nanoparticles would protect the steel reinforcement from chloride induced corrosion by forming a protective barrier.

5. REFERENCES

[1] Koch, G.K.; Brongers, P.M.; Thompson, G.; Virmani, P.; and Payer, J., "Corrosion Cost and Preventive Strategies in the United States," US Department of Transportation Federal Highway Administration, Report No FHWA-RD-01-156, March 2002, pp.3-9.

[2] Reinhardt, H.W., "Transport of Chemicals through Concrete," Materials Science of Concrete III, J.P. Skalny, Ed., American Ceramic Society, Westerville, 1992, pp.209-241.

[3] Samaha, H,R; and Hover, K,C., "Influence of microcracking on the mass transport properties of concrete," *American Concrete Institute Materials Journal*, Vol 89, April 1992, pp.416-424.

[4] Luping, T., Nilsson, L., "Rapid Determination of the Chloride Diffusivity in Concrete by Applying and Electrical Field," ACI Materials Journal, Paper Title No. 89-M6, pp.49-53, January-February 1993.

[5] M. Pigeon, R. Pleau, Modern concrete technology 4, Durability of Concrete in cold climates, Taylor & Francis, London, June 1995.

[6] Johansen, V., Goltermann, P., Thaulow, N., "Chloride Transport in Concrete," Concrete International, pp. 43-44 July, 1995.

[7] Huang, P., Bao, Y., Yao, Y., "Influence of HCl Corrosion on the Mechanical Properties of Concrete", Cement and Concrete Research, Vol. 35, No.3, pp584-589, March 2005.

[8] Jung, W.-Y., Yoon, Y.-S., Sohn, Y.-M., "Predicting the Remaining Service Life of Concrete by Steel Corrosion", Cement and Concrete Research, Vol. 33, No.5, pp. 663-678, May 2003.

[9] Jones, A.J., Principles and Prevention of Corrosion, Prentice Hall, New Jersey, 2nd Ed, 1995, pp.388-391.

[10] Johnson, W., "Cost-Effective Extraction of Chlorides form Bridge Steel," Journal of Protective Coatings and Linings, pp. 82-92, January 1997.

[11] Mindess, S., Young, J. F., Concrete, Prentice-Hall Inc., Englewood Cliffs, New Jersey, 1996.

[12] Taylor, p. 361, 1997 H.F.W. Taylor, 'Cement Chemistry', 2nd edn, 132-134,1997 London, Thomas Telford Publishing.

[13] Xypex, "Concrete Waterproofing by Crystallization", Data Sheet 005, Richmond B.C., Canada, 1983.

[14] Vandex, "Water Proofing Systems", Vandex product brochure, Stamford, CT, 1983.

[15] Finney, D., "Electro-osmosis Dries Wet Areas", Cutting Edge, USACERL, Champaign, IL, 1998.

[16] Hock, V., McInerney, M. K., Kirstein, E., "Demonstration of Electro-Osmotic Pulse Technology for Groundwater Intrusion Control in Concrete Structures," US Army Facilities Engineering Applications Program Technical Report 98/86, p.19, 1998.

[17] Bakker, R.F.M., "On the Cause of Increased Resistance of Concrete made from Blastfurnace Cement to the Alkali-Silica Reaction and to Sulfate Corrosion", Thesis, TH-Achen, Aachen, Federal Republic of Germany, 1980.

[18] Lagerblad, B., Jennings, H.M., and Chen, J., "Modification of Cement Paste with Silica Fume-A NMR Study", 1st International Symposium on Nanotechnology in Construction, Paisley, Scotland, pp. 123-131, 2003.

[19] Bhanja, B. Sengupta, Influence of silica fume on the tensile strength of concrete, Cem. Concr. Res. 35 (4), (2005), 743-747.

[20] S. Chandra, Y. Ohama, Polymers in Concrete, CRC Press, Boca Raton, FL, pp 210-341, 1994. [21] Nelson *et al.*, (1977)

[22] I. Campillo, J. S. Dolado, A. Porro, High-performance nanostructured materials for Construction, 1st International Symposium on Nanotechnology in Construction, Paisley, Scotland, (2003), 215-225.

[23] W. Ortlepp, "Electroosmotic process for coating and impregnating nonmetallic, non-Conductive porous materials with and inorganic and/or organic binder," German Patent CA Section 42 (Coatings, links and Related Products) DE 4113942, October 1992.

[24] Gratwick, R. T., Dampness in Buildings, John Wiley & Sons, New York, 1974.

[25] Otsuki, N., Hisada, M., Ryu, J., Banshoya, E., "Rehabilitation of Concrete Cracks by Electrodeposition", Concrete International, pp. 58-63, March 1999.

[26] Ryu, J., Otsuki, N., "Crack Closure of Reinforced Concrete by Electrodeposition Technique," Cement and Concrete Research, Vol. 32, No. 1, pp. 159-164, January 2002.

[27] Kasselouri, V., Kouloumbi, N., Thomopoulos, Th., "Performance of Silica Fume-Calcium Hydroxide Mixture as a Repair Material", Cement and Concrete Composites, Vol. 23, No. 1, pp. 103-110, 2001.

[28] Sloane, N.J.A. "The Sphere Packing Problem", Doc.Math.J.DMV, Documenta Mathematica Extra Volume ICM 1998.

[29] Lagarias, J.C., C.L.Mallows and A.R.Wilks,"Beyond the Descartes Circle Theorem", Amer. Math. Monthly,Vol.109, No.4, 2004, pp.338-361.

[30] Jensen, F. *Introduction to Computational Chemistry*; Wiley: Chichester, 1999.

[31] Koch, W.; Holthausen, M. C. *A Chemist's Guide to Density Functional Theory*, Second ed.; Wiley-CVH, 2001.

[32] Hehre, W. J.; Radom, L.; Schleyer, P. v. R.; Pople, J. A. *Ab Initio Molecular Orbital Theory*; John Wiley & Sons: New York, 1986.

[33] *Recent Developments and Applications of Modern Density Functional Theory*; Seminario, J. M., Ed.; Elsevier Science Publishers: Amsterdam, 1996; Vol. 4.

[34] Parr, R. G.; Yang, W. *Density Functional Theory of Atoms and Molecules*; Oxford University Press: Oxford, 1989.

[35] Wolfram, K.; Holthausen, M. C. *A Chemist's Guide to Density Functional Theory*, Second ed.; Wiley-VCH: New York, 2000.

[36] Foresman, J. B.; Frisch, A. *Exploring Chemistry with Electronic Structure methods*, 2nd. edition ed.; Gaussian, Inc.: Pittsburgh, 1996.

[37] Broadbelt, L. J.; Snurr, R. Q. *Appl. Cat. A* 2000, *200*, 23.

[38] Perdew, J. P.; Wang, Y. *Phys. Rev. B* 1992, *45*, 13244.

[39] Ensing, B.; Meijer, E. J.; Blöchl, P. E.; Baerends, E. J. *J. Phys. Chem. A* 2001, *105*, 3300.